# SUPERCONDUCTING CAVITY DEVELOPMENT FOR HIGH INTENSITY PROTON LINAC IN JAERI

N. Akaoka, E. Chishiro, K. Hasegawa, M. Mizumoto, J. Kusano, N. Ouchi#, JAERI, Tokai-mura, Ibaraki-ken, 319-1195, Japan, H. Inoue, E. Kako, S. Noguchi, M. Ono, K. Saito, T. Shishido, KEK, Tsukuba-shi, Ibaraki-ken, 305-0801, Japan, K. Mukugi, C. Tsukishima, MELCO, Kobe-shi, Hyogo-ken, 652-8555, Japan, O. Takeda, Toshiba Corporation, Yokohama-shi, Kanagawa-ken, 230-0045, Japan, M. Matsuoka, MHI, Yokohama-shi, Kanagawa-ken, 220-8401, Japan

*Abstract*

The JAERI/KEK Joint Project based on a high intensity proton accelerator is planned. Superconducting cavities are intended to apply to the high energy part of the linac. System design of the SC linac for the Joint Project has been carried out on the basis of a design for the JAERI original project. In the R&D work for superconducting cavities, vertical tests of single-cell and 5-cell cavities, pretuning of 5-cell cavities were carried out. A model describing dynamic Lorentz detuning has been newly established. Validity of the model was confirmed experimentally. This paper describes the system design of the SC proton linac, present status of the R&D work and the new model for the dynamic Lorentz detuning.

## 1 INTRODUCTION

Japan Atomic Energy Research Institute (JAERI) proposed the Neutron Science Project (NSP) for the investigations in the fields of basic science and nuclear technology by using of the high intensity proton accelerator[1]. The accelerator was designed to be a 1.5-GeV linac and two storage rings, and the maximum beam power was intended to be 5 MW. Superconducting (SC) structure was chosen for the high energy part of the linac from 0.1 to 1.5 GeV[2].

High Energy Accelerator Research Organization (KEK) also planned the Japan Hadron Facility (JHF) for neutron science, muon science, exotic nuclei science, fundamental particle physics and neutrino oscillation experiment[3]. It was planned that the JHF comprises a 50-GeV main synchrotron, a 3-GeV rapid-cycling synchrotron (RCS) and a 200-MeV linac.

In 1999, JAERI and KEK agreed each other to bring the NSP and the JHF into one joint project because both projects have some common features which are summarized in a single key word; “high power proton accelerators”[4]. Design work and R&D studies for the Joint Project are in progress. R&D studies for the SC proton linac based on the NSP is being continued in JAERI in collaboration with KEK. The R&D results contribute to the design of the Joint Project and the R&D target will be shifted toward the Joint Project.

In the NSP and the Joint Project, pulsed operation of the SC cavities is necessary. Therefore, dynamic behavior of the Lorentz detuning is important for stable RF control. Lorentz vibration model was established to describe dynamic behavior of the Lorentz detuning.

This paper describes the system design of the SC proton linac for the Joint Project, the present status of the R&D activities for SC cavities in JAERI, and investigation on the dynamic Lorentz detuning.

## 2 SC LINAC FOR THE JOINT PROJECT

### *2.1 Overview of the Joint Project*

Figure 1 shows a schematic view of the accelerator for the Joint Project. It consists of a 600-MeV linac, a 3-GeV RCS and a 50-GeV synchrotron. Fundamental particle, nuclear physics and neutrino experiments will be done by proton beams from the 50-GeV synchrotron. The neutron science, muon science and exotic nuclei science will be studied using proton beams from the 3-GeV RCS. R&D studies for the nuclear transmutation will be performed with proton beams from the linac.

The project is divided into two phases. In the first phase, 1 MW and 750 kW beam power will be achieved at the output of the 3-GeV RCS and the 50-GeV synchrotron, respectively. The 5 MW beam power for the neutron science is the final goal in the second phase. The upgrade

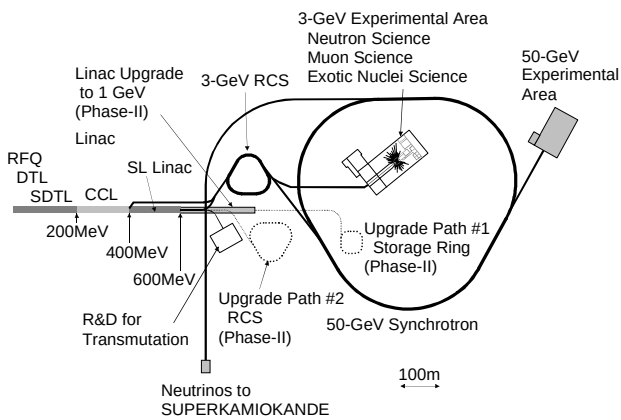


Fig. 1 Schematic view of the Joint Project

# E-mail: ouchi@linac.tokai.jaeri.go.jp

to Phase-II will be achieved with full-energy linac (1 GeV) and storage rings (upgrade path #1). Other upgrade path is also considered; upgrade the energy and current of the RCS and install one more RCS (upgrade path #2)[4].
The linac for Phase-I comprises a negative ion source, a 3-MeV RFQ, a 50-MeV DTL, a 200-MeV SDTL (Separated type DTL), a 400-MeV CCL and a 600-MeV SC linac. Frequency of RFQ, DTL and SDTL is 324 MHz. Frequency of the high energy section of CCL and SC linac is determined to be 972 MHz which means 3 times frequency jump at 200 MeV. Momentum spread of $\Delta p/p<0.1\%$ is required for the linac output beams to inject to the RCS, that is very important for design of the linac. It is planned that 400 MeV beams are injected to the RCS in the first commissioning, because beam study of the SC linac in the pulsed operation is necessary to provide acceptable beams for the RCS. In this period, the SC linac provides beams to the R&D for transmutation as well as the beam study, and then 600 MeV beams will be injected to the RCS.

## *2.2 System design of the SC linac*

Injection energy of the SC linac is 397 MeV and output energies at Phase-I and Phase-II are 600 MeV and 1 GeV, respectively. Reference design of the SC proton linac system from 397 MeV to 1 GeV have been performed.
Resonant frequency of SC cavities is 972 MHz. The number of cells per cavity and the maximum surface peak field ($E_{peak}$) of the cavities are determined to be 7 and 20 MV/m, respectively, by considering accelerator length, higher order mode effects, microphonics, coupler power and capital cost.
The SC proton linac should be divided into several cavity groups because proton velocities are increasing as accelerated. Too few groups cause low accelerating efficiency and emittance growth, and too many groups lead increase of fabrication costs. A scheme of "same phase slip at each cell [2]" has been adopted in the cavity grouping. We have chosen 6-group design, i.e., 3 groups between 397 and 600 MeV, and 3 more groups between 600 and 1000 MeV. In this design, the phase slip of the beam bunch in the 7-cell cavity is less than 10 deg., which provides high accelerating efficiency and low longitudinal emittance growth. Average synchronous phase angle was set to be –35 deg. in this design.

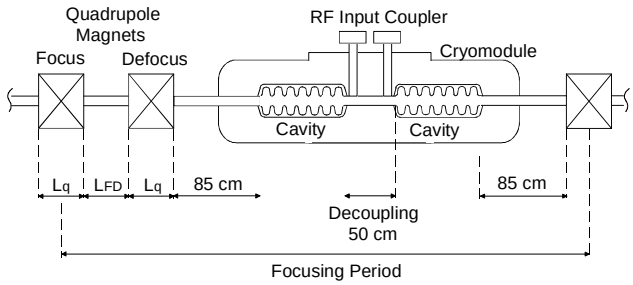


Fig. 2 Schematic view of lattice structure

Figure 2 shows the schematic view of lattice structure of the SC linac. The lattice design has been performed according to the equipartitioning scheme to reduce longitudinal emittance growth. Lengths of quadrupole magnets were determined from the limitation of Lorentz stripping of the negative hydrogen beams due to the magnetic field. Design criteria of 10% margin for the field gradient of stripping rate less than $10^{-8}$/m at bore radius (5cm) is adopted in this design. We also apply a criteria for lattice design that zero current transverse phase advance should be less than 90 deg. to avoid the envelope instability. Table 1 summarizes the design parameters. Quadrupole magnet length ($L_q$) and distance between magnets ($L_{FD}$) are 45 cm in the energy region up to 600 MeV. In the higher energy region, they become longer (47-55 cm) because of the limitation of the Lorentz stripping. The $E_{peak}$ values in the first group are less than 20 MV/m because of the limitation of envelope instability. If $E_{peak}$ field of 20 MV/m is applied for all of the cavities in the first group, transverse phase advances exceed 90 deg. to keep the equipartitioned condition. In the other groups, $E_{peak}$ values are also adjusted to achieve smooth phase advance between groups. Total lengths up to 600 and 1000 MeV are 109 and 281 m, respectively.

## *2.2 Beam simulation*

Beam simulation has been carried out using the modified PARMILA code. Figure 3 shows RMS emittance from 397 to 1000 MeV. Since the equipartitioning scheme has been applied in this design, emittance growth rates in both transverse and longitudinal direction are very small as shown in Fig. 3. The calculated RMS beam size in transverse direction is in the region between 0.8 to 1.8

Table 1 Design parameters for the SC linac

| Group No. | 1 | 2 | 3 | 4 | 5 | 6 |
|---|---|---|---|---|---|---|
| Energy (MeV) | 397-453 | 453-523 | 523-600 | 600-696 | 696-824 | 824-1000 |
| Particle β | 0.711-0.738 | 0.738-0.766 | 0.766-0.792 | 0.792-0.818 | 0.818-0.847 | 0.847-0.875 |
| Geometrical β ($\beta_g$) | 0.725 | 0.751 | 0.778 | 0.806 | 0.833 | 0.861 |
| $E_{peak}$ (MV/m) | 15-20 | 19.2-20 | 18.8-20 | 20 | 19.4-20 | 19.4-20 |
| $E_{acc}$ (MV/m) | 5.2-7.2 | 7.2-7.6 | 7.5-8.2 | 8.3-8.4 | 8.4-8.8 | 8.5-9.0 |
| No. of modules | 7 | 7 | 7 | 8 | 10 | 13 |
| $L_q$, $L_{FD}$ (cm) | 45 | 45 | 45 | 47 | 50 | 55 |
| Length (m) | 35.8 | 36.2 | 36.6 | 42.8 | 55.0 | 74.2 |

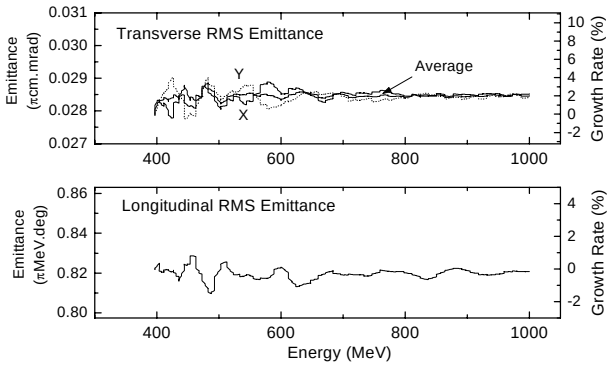


Fig. 3 RMS emittances obtained in the beam simulation

mm. As the bore radius is set to be 5 cm, the ratio of bore radius to RMS beam size is more than 28, which is considered to be enough to reduce beam loss in the linac.

It is planned that 600 MeV proton beams will be injected into the RCS in the Phase-I of the Joint Project. For the RCS injection, momentum spread of the beams should be less than ±0.1%, which refers to energy spread less than about ±1MeV. Effects of the RF control error have been evaluated in the energy region between 397 to 600 MeV. Phase and amplitude errors of the cavity field have been introduced independently in the simulation. These errors have uniform distribution in the range up to ±2deg. and ±2% for phase and amplitude, respectively. 1000 calculations were carried out in a given error condition and average output energy of the beam bunch in each calculation was dealt with statistically. Figure 4 shows histograms of the average output energy for phase and amplitude errors; energy spread of the beams becomes wider as the errors increase. We estimated the energy spread using the standard deviation of the histogram. Figure 5 shows the standard deviations as error bars as a function of amplitude and phase errors. In the cases of ±1deg. phase error and ±1% amplitude error, the standard deviations are $\sigma_{PHIerr}$ = ±0.23 MeV and $\sigma_{AMPerr}$ = ±0.19 MeV, respectively. Energy spread of the injected beam at 397 MeV was assumed to be $\sigma_{injector}$ = ±0.2 MeV. We assumed that these energy spreads cause independently and

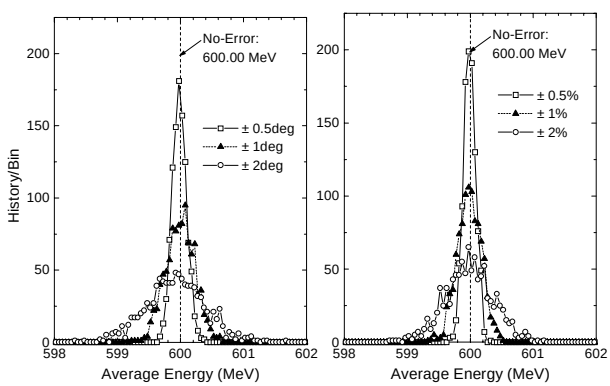


Fig. 4 Histograms of the average output energy obtained by 1000 calculations in each error condition

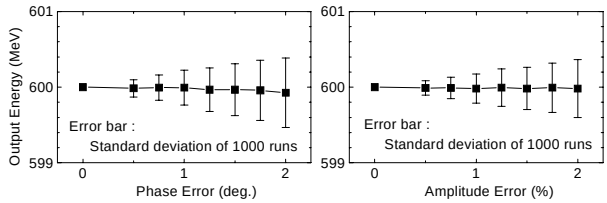


Fig. 5 Energy spread of the beams obtained in the error analysis

evaluated total energy spread.

$$\sigma = \sqrt{\sigma_{injector}^2 + \sigma_{PHIerr}^2 + \sigma_{AMPerr}^2} = \pm 0.36 \text{ MeV}$$

Required energy spread, ±1 MeV, is approximately same as 3σ. Therefore, we considered that the error tolerance of the RF control is less than ±1deg. in phase and ±1% in amplitude. In addition to the RF control error, we should consider intrinsic energy spread, 0.2 MeV, after debunching without any errors.

## 3 SC CAVITY DEVELOPMENT

SC cavity development is continued on the basis of the JAERI original project (NSP). In this development work, vertical tests of a single-cell cavity (β=0.886), pretuning of 5-cell cavities (β=0.5 and 0.886) and vertical test of 5-cell cavity (β=0.5) have been carried out.

### *3.1 Vertical tests of a single-cell cavity (β=0.886)*

A single-cell cavity of β=0.886 was fabricated in the KEK workshop. Figure 6 illustrates cross sectional view of the cavity. Resonant frequency, $E_{peak}/E_{acc}$ ratio and geometrical factor of the cavity are 594.2 MHz, 2.0, and 236 Ω, respectively.

Surface treatment of barrel polishing (BP) and electropolishing (EP1), heat treatment at 750 °C for 3 hours, and high pressure water rinsing (HPR) at 8-9 MPa for 1.5 hours were applied in this cavity. After these processing, the first vertical test was performed. Average

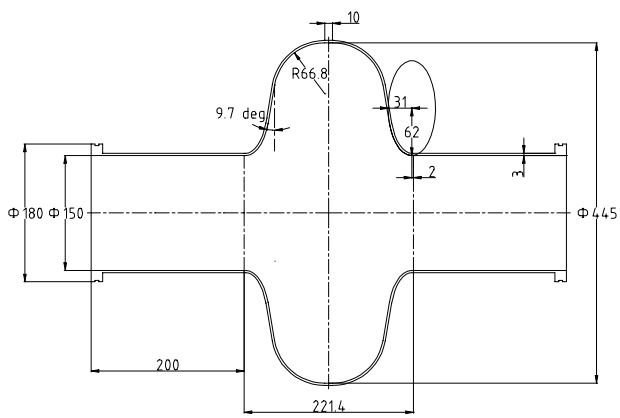


Fig. 6 Cross sectional view of a single-cell cavity (β=0.886)

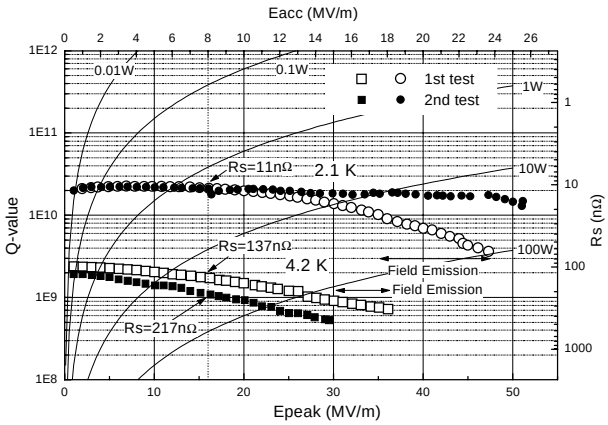


Fig. 7 Vertical test results of a single-cell cavity (β=0.886)

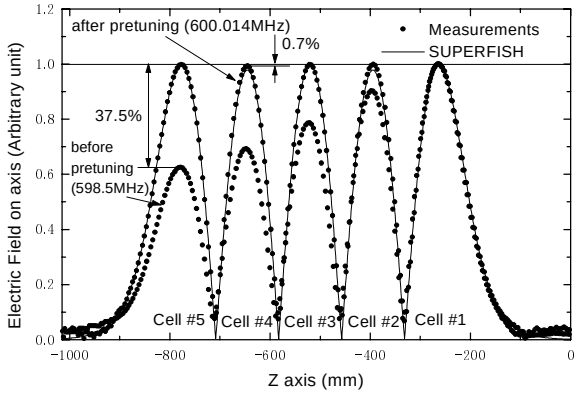


Fig. 9 Field distribution on axis of the 5-cell copper model cavity (β=0.5) before and after pretuning

removal thicknesses in BP and EP1 were 124 μm and 31 μm, respectively. After the first test, additional electropolishing (EP2 : 30μm), HPR and the second vertical test were carried out.

Figure 7 show the $Q_0$-$E_{peak}$ curves obtained in the vertical tests. The measurements were performed at 4.2K and 2.1K in the both tests. In the first test, $E_{peak}$ value of 47.2 MV/m was achieved at 2.1K. At 4.2K, $E_{peak}$ value reached 36 MV/m, where the limitation was the output power of the RF amplifier. The maximum field strengths obtained in these tests were much higher than the design field strength in the NSP (16MV/m). Quality factors at low field region were $2\times10^{10}$ and $2\times10^{9}$ at 2.1 and 4.2K, respectively. Field emission was observed in the high field measurements. In the second test, field emission was observed even in the low field measurement. However, it was processed at $E_{peak}$ of ~16 MV/m in the 2K measurement and was reduced much much in the higher field region. The reason of the field emission is considered to be impurity of the water used in the HPR. The maximum $E_{peak}$ values were 51 and 29.5 MV/m at 2 and 4.2K, respectively. Quality factor at 2K was about $2\times10^{10}$ which was the same as the first measurement and was kept in the high field region. However, quality factor at 4.2K was in the range between $5\times10^{10}$ and $2\times10^{9}$ which were less than those in the first measurement.

### *3.2 Pretuning of 5-cell cavities (β=0.5, 0.886)*

Two 5-cell cavities of β=0.5 were fabricated in the KEK workshop; one is a copper model cavity and the other is a niobium cavity. Figure 8 illustrates the shape of 5-cell cavity. Frequency, $E_{peak}/E_{acc}$, $H_{peak}/E_{acc}$, R/Q and

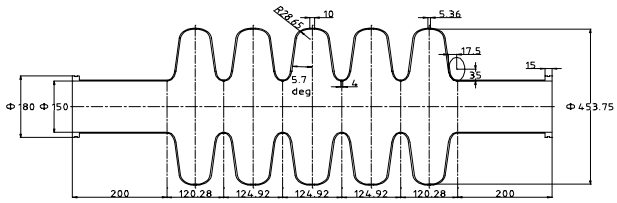


Fig. 8 Shape of 5-cell cavity (β=0.5)

geometrical factor of the cavity are 600 MHz, 4.67, 94.8 Oe/(MV/m), 77.1Ω and 137 Ω, respectively. Equator straight lengths at both end cells are adjusted to achieve flat electric field distribution on the beam axis. Pretuning of these cavities have been carried out.

Figure 9 shows the relative electric field on beam axis measured by bead perturbation method for the copper cavity before and after the pretuning. The calculated result by the SUPERFISH code is also presented in Fig. 9. Maximum deviation of the peak field at each cell center was 37.5% before the pretuning. After the pretuning, the deviation was improved within 0.7% and the agreement of the measured data with the calculated data is quite well. Frequency error of the cavity was also improved from -1.5 MHz to +14 kHz.

In the case of the niobium cavity, we had a trouble in fabrication; the final electron beam welding at iris between cell #3 and #4 made hole because the cavity rotation was not smooth. The hole was repaired and welding was repeated several time to make complete seam. As the result of this trouble, iris between cell #3 and #4 became narrower compared to the designed shape. We tried to force pretuning of this cavity and the shape was deformed very much. Figure 10 shows the electric

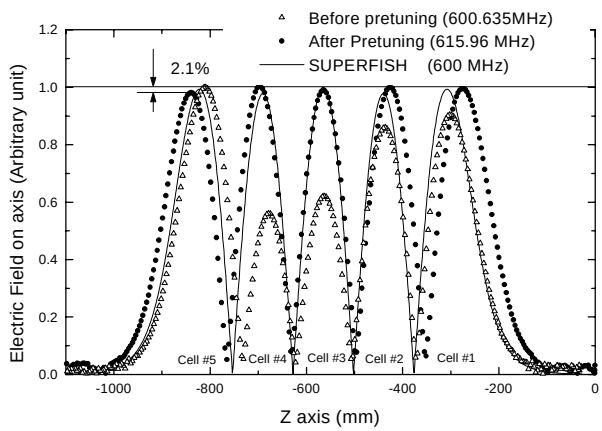


Fig. 10 Field distribution on axis of the 5-cell niobium cavity (β=0.5) before and after pretuning

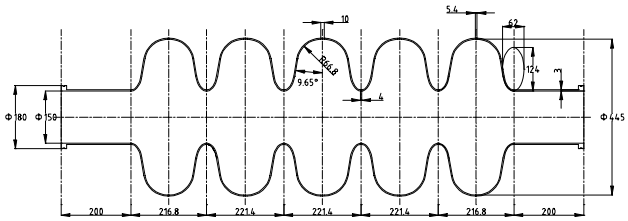

Fig. 11 Shape of 5-cell cavity (β=0.886)

field distributions before and after the pretuning compared to those obrained by the calculation. Field flatness within 2.1% was achieved after the pretuning but cavity length became longer by about 6 cm and frequency increased by about 16 MHz.

Two 5-cell cavities of β=0.886 made of copper and niobium were also fabricated in Toshiba corporation. Figure 11 illustrates the cross sectional view of the cavity. Frequency, $E_{peak}/E_{acc}$, $H_{peak}/E_{acc}$, R/Q and geometrical factor of the cavity are 600 MHz, 2.04, 47.4 Oe/(MV/m), 443 Ω and 235 Ω, respectively. Pretuning of the copper model cavity was carried out. Figure 12 shows the field distributions before and after pretuning. Field flatness was improved from 38.4% to 1.3% in the pretuning. Pretuning of the niobium cavity is in preparation now and will be done in a few months.

### *3.3 Vertical test of 5-cell cavity (β=0.5)*

Surface treatment and vertical test of the 5-cell niobium cavity (β=0.5) were carried out. The same procedure of the surface treatment as the single-cell cavity of β=0.886, i.e., barrel polishing (BP) and electropolishing, (EP) was applied in this cavity. Average removal thickness in BP and EP were 97 μm and 30 μm, respectively. After the surface treatment, heat treatment at 750 °C for 3 hours and HPR for 1.5 hours were done before vertical test.

Figure 13 shows the result of the vertical test of the 5-cell cavity. Maximum field strengths of 17.3 and 18.7 MV/m were achieved in 2K and 4.2K measurements, respectively. The limitations of the field were quench and RF power at 2K and 4.2K, respectively. These field

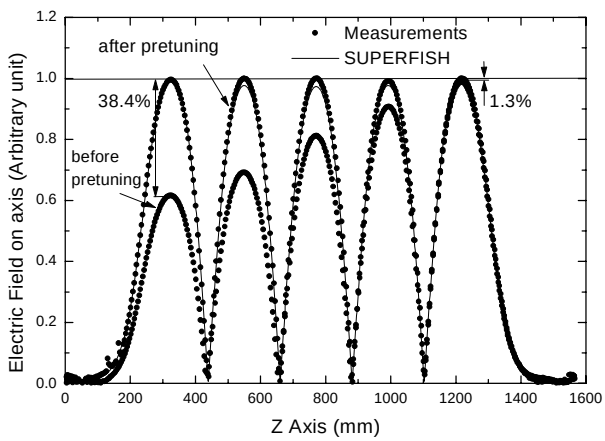


Fig. 12 Field distribution of the 5-cell copper model cavity (β=0.886) before and after pretuning

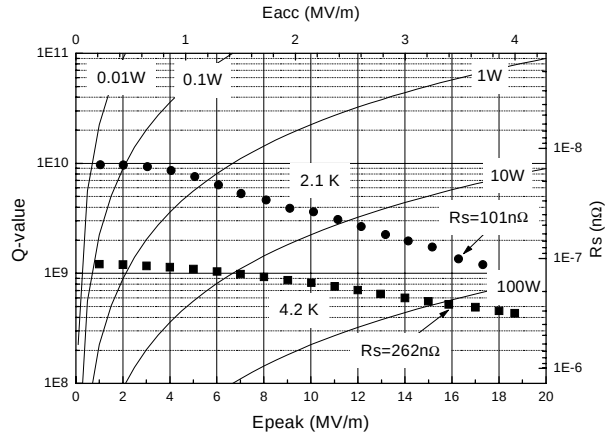


Fig. 13 Vertical test results of a 5-cell cavity (β=0.5)

strengths exceed design values of 16 MV/m but much lower than those obtained in the single-cell cavity tests[5]. Quality factors were reasonable at low field strength ($1\times10^{10}$ and $1\times10^{9}$ at 2K and 4.2K, respectively), but were degraded as field increase. Surface resistance values at 16 MV/m were 101 nΩ and 262 nΩ at 2K and 4.2K, respectively. The cavity performance was not good compared to the single-cell cavities, that is considered due to the cavity deformation in the pretuning described in Sec. 3.2, and insufficient surface treatment as a result of the deformation.

## 4 DYNAMIC ANALYSIS OF LORENTZ DETUNING

In the Joint Project, pulsed operation of the SC cavities is planned; repetition rate of 50Hz and beam pulse length of 0.5-2 ms. Dynamic behavior of the Lorentz detuning due to the pulsed operation is very important for stable RF control of the cavities. Lorentz vibration model was established to simulate RF control of the cavity including dynamic Lorentz detuning.

### *4.1 Dynamic analysis of Lorentz detuning by structural analysis code*

In the first step of the investigation, we performed dynamic analysis of the Lorentz detuning using the FEM code “ABAQUS”. Figure 14 shows shape of a model used in the analysis as well as deformed shape by the stationary Lorentz force. The model was axisymmetric

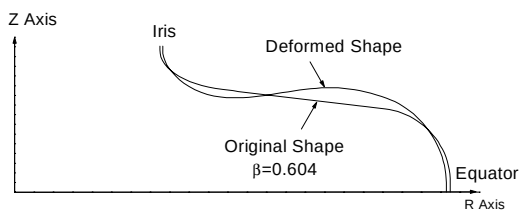


Fig. 14 Cavity model used in the dynamic Lorentz detuning and deformed shape by the stationary Lorentz force

half-cell geometry of 600 MHz cavity and the geometrical β was 0.604. Fixed constrained condition in the Z-direction was applied for both ends, iris and equator. The Lorentz force on the cavity wall was deduced from the electromagnetic field distribution obtained by the SUPERFISH code. Dynamic deformation of the model in each time step was calculated by modal analysis method using the ABAQUS code and was converted to frequency shift using frequency sensitivity data by the SUPERFISH code.

Figure 15 shows an example of the dynamic analysis result. In this analysis, cavity wall thickness was 4.8 mm, mechanical quality factor ($Q_m$) was 100, and cavity field increased linearly in 2 ms, held for 2 ms and decreased linearly in 2 ms. The result indicates that the Lorentz detuning reacts very quickly and vibrates in the flat top and after the RF pulse. In this modal analysis, 10 mechanical modes were considered and we found that the first 3 modes dominates the dynamic deformation by the Lorentz force. These 3 mechanical modes are shown in Fig. 16. Thus, the vibration in Fig. 15 has 3 frequency components corresponding to these 3 mechanical modes.

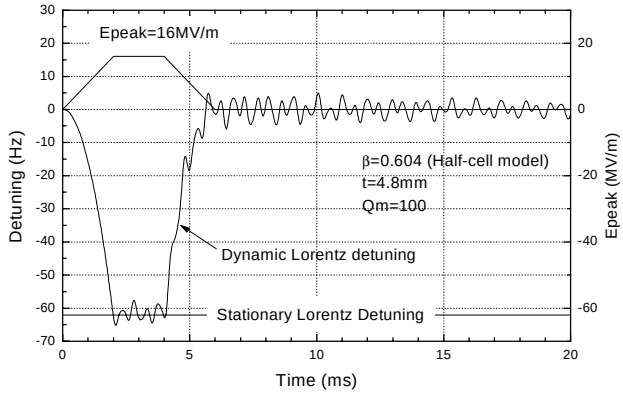


Fig. 15 Example of the dynamic analysis result

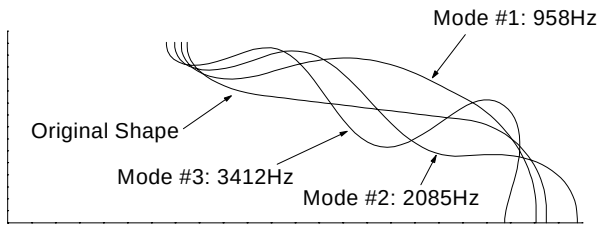


Fig. 16 First 3 mechanical modes of the half-cell

## 4.2 *Lorentz vibration model*

The Lorentz detuning and the cavity field affect each other. Therefore, the dynamic Lorentz detuning and the dynamic cavity field have to be solved simultaneously in order to simulate RF control of the cavity field. Such method is impossible in the method described above because the structural code requires time-dependent Lorentz force, i.e., cavity field, before the calculation.

To solve the dynamic Lorentz detuning and the dynamic cavity field simultaneously, we established Lorentz vibration model which describes dynamic behavior of the Lorentz detuning as follows [6,7].

$$\frac{d^2\Delta f_k}{dt^2}+\frac{\omega_{mk}}{Q_{mk}}\frac{d\Delta f_k}{dt}+\omega_{mk}^2\Delta f_k = K_k\left(\frac{V_C}{V_0}\right)^2 \qquad (1)$$

$$K_k=\frac{1}{m_k}\left\{\left(\frac{\vec{df}}{du}\right)\bullet\left(\vec{a}_k\right)\right\}\left\{\left(\vec{F}_0\right)\bullet\left(\vec{a}_k\right)\right\}$$

$$\Delta f=\sum_k \Delta f_k$$

*where*

$V_c$ : cavity voltage (V)
$k$ : mechanical vibration mode number
$\Delta f_k$ : detuning for k - th mode (Hz)
$\Delta f$ : total detuning (Hz)
$\omega_{mk}$ : angular frequency for $k$ - th mechanical mode (rad / s)
$Q_{mk}$ : quality factor for $k$ - th mechanical mode
$m_k$ : generalized mass for $k-th$ mechanical mode (kg)
$\vec{F}_0$ : Lorentz force vector at cavity voltage of $V_0$ (N)
$\vec{a}_k$ : eigenvector for $k-th$ mechanical mode
$\vec{df}/du$ : frequency sensitivity vector for displacement (Hz / m)
$u$ : cavity wall displacement (m)

The inner products of $(df/du)\bullet(a_k)$ and $(F_0)\bullet(a_k)$ mean the frequency sensitivity of *k-th* mechanical mode and contribution of the Lorentz force to the *k-th* mechanical mode. ($F_0$) and (df/du) can be calculated by the electromagnetic analysis code (SUPERFISH), and $\omega_{mk}$, $m_k$ and $a_k$ can be obtained by the structural analysis code (ABAQUS).

The equation (1) was applied to solve the same problem as described in Sec. 4.1. A programming language of MATLAB/Simulink was used to solve the double differential equation (1). Figure 17 shows the result by the Eq. (1) compared with that by the modal analysis with the ABAQUS code. An agreement of the result by the Lorentz vibration model with that by the modal analysis with the ABAQUS code is excellent as shown in Fig. 17. Therefore, it is confirmed that the Lorentz vibration model is equivalent to the modal analysis using the

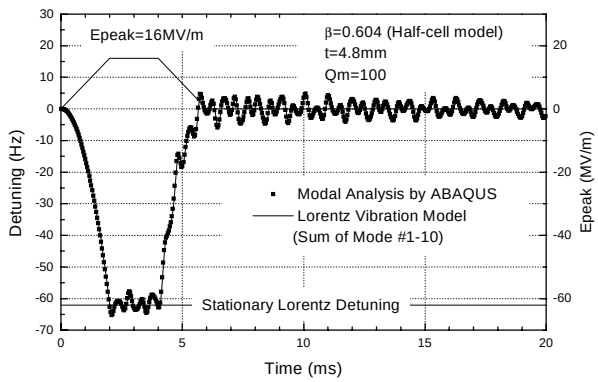


Fig. 17 Comparison of results by the Lorentz vibration model and the modal analysis with the ABAQUS code

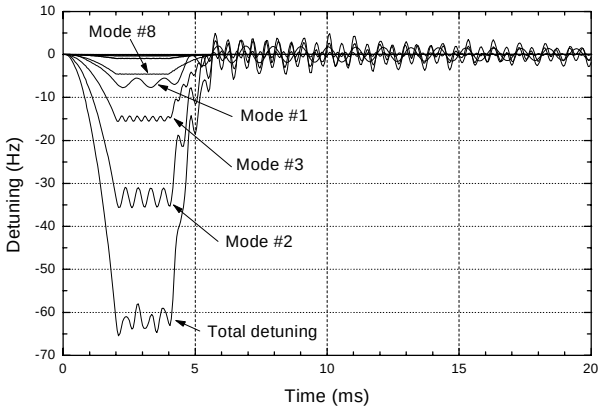


Fig. 18 Detuning for each mechanical mode and the total detuning obtained by the Lorentz vibration model

structural analysis code. In the Lorentz vibration model, contribution of each mechanical mode to the cavity detuning is derived. Figure 18 shows the detuning for each mechanical mode and the total detuning. It is clear that mode #1-3 and #8 dominate the detuning in this case.

### *4.3 Pulsed operation in the vertical test*

In order to observe the detuning vibration experimentally, a pulsed operation was carried out in the vertical test. A cavity used in the test was the single-cell cavity of $\beta$=0.886 described in Sec. 3.1. In this test, one side of cavity flange was fixed to the cryostat and the other side was free. As a result of this constrained condition, mechanical vibration mode of very low frequency was excited even in the slow and long pulsed operation at the vertical test. The measurement was made at 4.2 K. External quality factor of the input coupler was about $9\times10^7$.

Figure 19 shows RF power control signal, which is proportional to the RF amplifier output (max. 300W), and $E_{peak}$ in a pulse. Rise time, flat top and repetition rate of the pulsed operation were 60 ms, 100 ms and 0.76 Hz, respectively. The slow and long pulsed operation was due to the high loaded-Q and low RF power in the vertical test

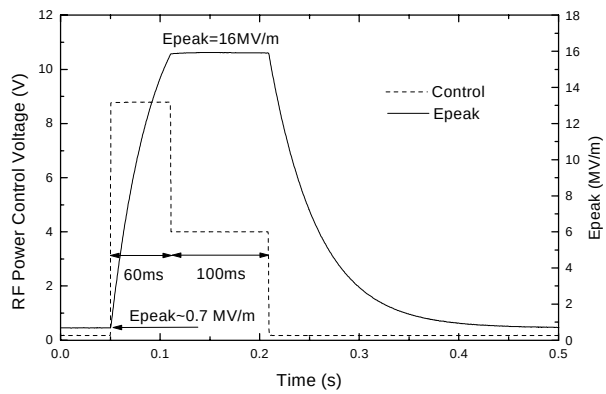


Fig. 19 RF power control signal and $E_{peak}$ in the pulsed operation

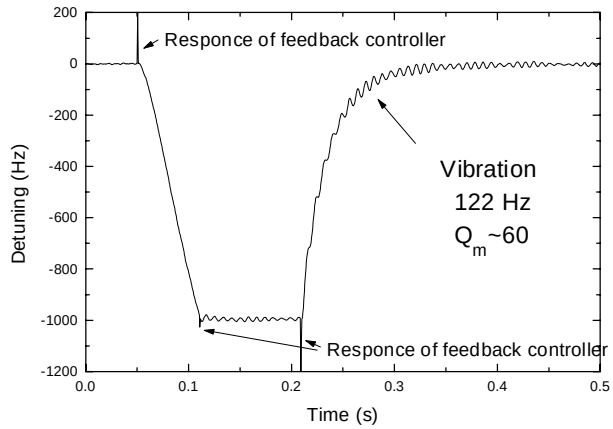


Fig. 20 Dynamic Lorentz detuning measured in the pulsed operation

system. Low RF power was fed to the cavity between the pulses in order to keep lock of PLL (phase locked loop) circuit. Cavity field strength at beginning of the pulse was $E_{peak}$~0.7 MV/m; this effect to the dynamic Lorentz detuning was negligibly small. Dynamic Lotentz detuning was measured by taking a FM control signal of PLL circuit through a low path filter of 1 kHz. The signal was accumulated for about 40 pulses and averaged in order to eliminate random noises.

Figure 20 shows the dynamic Lorentz detuning obtained in this test. Vibration of the detuning was observed at the flat top and decay of the pulse as expected. Impulses at the beginning of the rise, and both ends of the flat top were response of a feedback controller used in the PLL circuit. Frequency and quality factor of the vibration were estimated to be 122 Hz and about 60 by analyzing the waveform at the decay.

The Lorentz vibration model of Eq. (1) was applied for the simulation of the pulsed operation. In order to prepare parameters the SUPERFISH and the ABAQUS calculations were carried out and we found that the first mechanical mode dominates the deformation. Figure 21 shows the first mechanical mode. The frequency of the mode was calculated to be 111 Hz, which agreed well with the frequency of the detuning vibration obtained

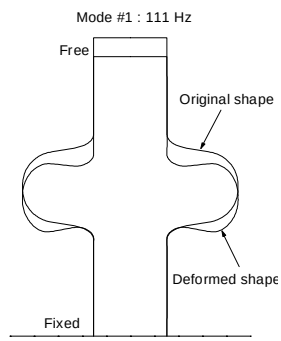


Fig. 21 First mechanical mode of the cavity

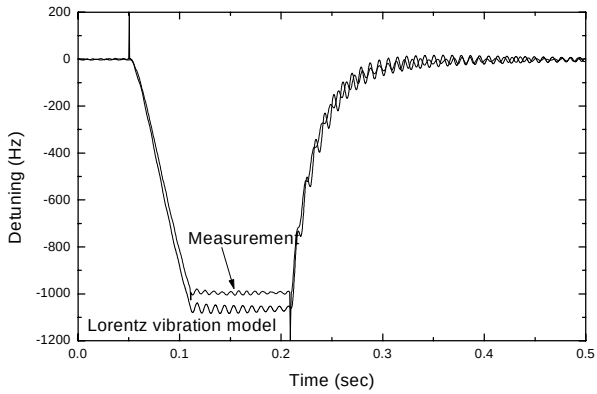


Fig. 22 Comparison between the Lorentz detuning obtained by the measurement and the Lorentz vibration model

experimentally, 122 Hz. In this simulation, parameters of $V_o$ and $Q_m$ in Eq. (1) were prepared from the experimental data; $E_{peak}$ data shown in Fig. 19 and $Q_m$=60, respectively. Figure 22 shows the simulation result compared with that by experiment. Average detuning frequencies at the flat top obtained in the measurement and the simulation agreed within 10 %. Behaviour of the vibration at the flat top and the decay obtained in the simulation is similar to that by the measurement. The model of this problem is very simple and the agreement between the measurement and the simulation indicates that the Lorentz vibration model describes dynamic behaviour of the Lorentz detuning in the pulsed operation.

Insignificant disagreement between the measurement and the simulation shown in Fig. 22 is considered due to errors of data used in the simulation, i.e., elastic modulus of niobium, thickness of the cavity wall and cavity shape as well as the measurement error of the field strength of the cavity. In applying the Lorentz vibration model, parameters of $\omega_1$ and $K_1$ (only the first mode dominates the detuning in this problem) were modified so as to reproduce the experimental data. $\omega_1$ was set to be $2\pi\times122$ (rad/sec) and $K_1$ was set so that the average detuning at the flat top became same as the measured data. Figure 23 shows the comparison between the modified simulation results and the experimental data at the flat top region. The agreement between the modified simulation and the measurement becomes very good.

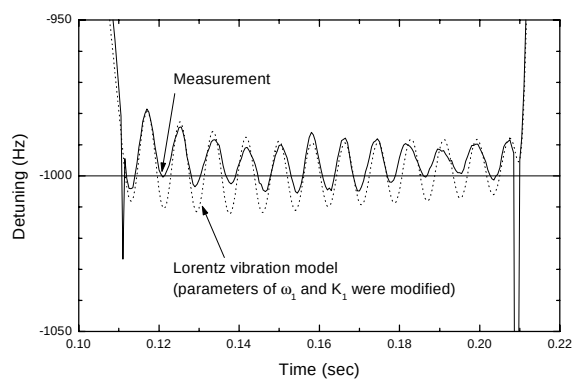


Fig. 23 Comparison between the modified simulation and the measurement at the flat top region

### *4.4 RF control simulation including dynamic Lorentz detuning*

The Lorentz vibration model was applied to a simulation of an RF control of the cavity. Dynamic cavity voltage ($V_c=V_{re}+jV_{im}$) is described by the two-coupled first order differential equations as follows[8].

$$\frac{d}{dt}\begin{bmatrix}V_{re}\\V_{im}\end{bmatrix}=\begin{bmatrix}-\omega_{1/2} & -\Delta\omega\\ \Delta\omega & -\omega_{1/2}\end{bmatrix}\begin{bmatrix}V_{re}\\V_{im}\end{bmatrix}+\omega_{1/2}\begin{bmatrix}R_L I_{re}\\R_L I_{im}\end{bmatrix} \quad (2)$$

where

$\omega_{1/2}$ : 3dB band width of the cavity

$\Delta\omega = 2\pi\left(\Delta f_{pre} + \Delta f\right)$

$\Delta f_{pre}$ : pre - detuning of the cavity

$R_L = \frac{1}{2}(R/Q)\bullet Q_L$

$I = I_{re} + jI_{im} = I_g + I_b$

$I_g$ : generator current

$I_b$ : twice of beam current

$V_g = R_L I_g$ : generator voltage

$V_b = R_L I_g$ : beam induced voltage

Equations (1) and (2) are coupled by $V_c$ and $\Delta f$ and solved simultaneously.

RF parameters used in this simulation are summarized in Table 2. Loaded quality factor ($Q_L$) was obtained by the optimum coupling of an input coupler for the beam

Table 2 RF parameters for the RF control simulation

| | |
|---|---|
| Frequency | 600 MHz |
| β | 0.604 |
| No. of cells | 5 |
| $E_{peak}$ | 16 MV/m (at flat top) |
| $V_c$ | 3.01 MV (at flat top) |
| Beam current | 28 mA ($I_b$ = 56 mA) |
| Synchronous phase $\phi_s$ | -30 deg. |
| Beam pulse length | 0.5 ms |
| $Q_0$ | 1.11E10 |
| $Q_L$ | 1.08E6 |
| R/Q | 115.39 Ω/cavity |
| Cavity wall thickness | 3 mm |

Table 3 Lorentz vibration parameters for the RF control simulation

| Mode No. k | 1 | 2 | 3 | 4 |
|---|---|---|---|---|
| $\omega_{mk}$ (k rad/s) | 3.63 | 10.0 | 15.4 | 21.6 |
| $m_k$ (kg) | 1.34 | 1.53 | 1.71 | 1.55 |
| $Q_{mk}$ | 100 | 100 | 100 | 100 |
| {df/du}•{$a_k$} (MHz/m) | 3.29 | -7.28 | -6.18 | 0.98 |
| {$F_0$}•{$a_k$} | -436 | 2150 | 1820 | -64.5 |

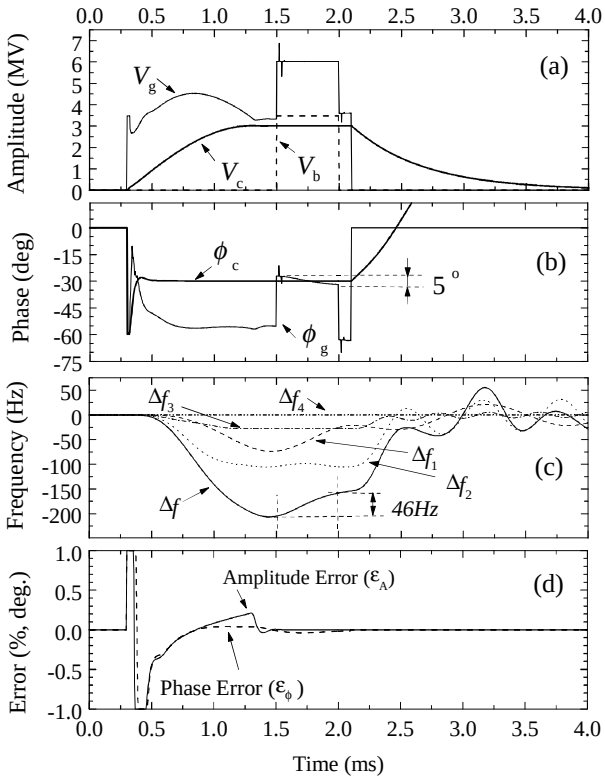


Fig. 24 Result of the RF control simulation including dynamic Lorentz detuning

loading. Pre-detuning ($\Delta f_{pre}$) was set so as to minimize RF power during the beam acceleration. Parameters for the Lorentz vibration model are listed in Table 3. These parameters were obtained half-cell geometry because we found multi-cell effect for the detuning was small compared to the single-cell contribution in the condition that both ends of the cavity were constrained. In this simulation, the first 4 mechanical modes, which dominated the detuning as shown in Fig. 18, are considered.

In the simulation, feedback and feedforward control was applied. Details of the control method is presented in [6]. Figure 24 shows the results of the simulation. The cavity voltage, $V_c$, was raised slowly in 1.2 ms in order to reduce the detuning vibration at the flat top. Maximum detuning was about 200 Hz at the beginning of the beam pulse and the detuning decreased by 46 Hz in the beam pulse of 0.5 ms. The detuning change led phase shift and feedback control stabilized cavity phase ($\phi_c$) by changing the generator phase ($\phi_g$) by 5 deg. within the beam pulse. As the result of the feedback and feedforward control, amplitude and phase errors within the beam pulse were less than 0.1% and 0.1 deg.

## 5 SUMMARY

System design of the SC proton linac has been carried out for the JAERI/KEK Joint Project. R&D work of the SC cavities for the high intensity proton linac is in progress step by step. The target of R&D work will be shifted from the NSP to the Joint Project. A model which describes the dynamic Lorentz detuning in the pulsed operation was newly established. The model was applied to the simulation of the RF control successfully.

Design of a prototype cryomodule, which includes two 5-cell cavities of $\beta$=0.604, is in progress. Fabrication of the cryomodule will be finished in 2000. Cavity and cryomodule tests will be done in that year. Experiments of the RF control is planned using the prototype cryomodule.

## 6 REFERENCES

[1] M. Mizumoto et al., “A High Intensity Proton Linac Development for the JAERI Neutron Science Project”, Proc. Linac98., Chicago, USA, (1998) in press,

[2] N. Ouchi et al., “Proton Linac Activities in JAERI”, Proc. 8th Workshop on RF Superconductivity, Abano Terme (Padova), Italy, p12 (1997)

[3] Y. Yamazaki, “ The Japan Hadron Facility Accelerator”, Proc. APAC98., Tsukuba, Japan, p314 (1998)

[4] Y. Yamazaki et al., “Accelerator Complex for the Joint Project of KEK/JHF and JAERI/NSP”, PAC99, New York, USA, p513 (1999)

[5] N. Ouchi et al., “Development of Superconducting cavities for High Intensity Proton Accelerator in JAERI”, IEEE Trans. on Applied Superconductivity, vol. 9, No. 2, p.1030 (1999)

[6] E. Chishiro et al., “Study of RF Control System for Superconducting Cavity”, Proc. of 12th Symposium on Accelerator Science and Technology in Japan (1999) in press

[7] C. Tsukishima et al., “Modelling of a super-conducting cavity de-tuning by the Lorentz pressure”, Proc. of 12th Symposium on Accelerator Science and Technology in Japan (1999) in press

[8] T. Shilcher et al., “Vector Sum control of Pulsed Accelerating Fields in Lorentz Force Detuned Superconducting Cavities”, TESLA report TESLA 98-20 (1998)